



Contents lists available at ScienceDirect

## Journal of Fluids and Structures

journal homepage: [www.elsevier.com/locate/jfs](http://www.elsevier.com/locate/jfs)

# Vortex-induced vibrations of an elastic cylinder near a finite-length plate

Oleg Ivanov<sup>a,\*</sup>, Vasily Vedeneev<sup>b</sup>

<sup>a</sup> Institute of Mechanics, Lomonosov Moscow State University, 1, Michurinskiy propsekt, Moscow, Russia

<sup>b</sup> Faculty of Mechanics and Mathematics, Lomonosov Moscow State University, GSP-1, Leninskie Gory, Moscow, Russia



## ARTICLE INFO

### Article history:

Received 4 August 2020

Received in revised form 6 September 2021

Accepted 13 September 2021

Available online xxxx

### Keywords:

Vortex-induced vibration

Vortex shedding

Cylinder near a plane boundary

Gap ratio

## ABSTRACT

In this study, vortex-induced vibrations of an elastic cylinder near a finite-length plate were experimentally investigated. A rubber cylinder of diameter  $D$  was spanned in a test section of a wind tunnel near a rigid plate of length  $\approx 6D$ . The oscillation amplitude peak for an isolated cylinder was  $0.3D$ , and the Reynolds number of the peak-amplitude regime based on cylinder diameter was in the range of 180–260. For a cylinder located sufficiently upstream relative to the plate trailing edge, it was found that oscillation amplitude ratio  $A/D$  decreased if the gap ratio  $G/D$  between the cylinder surface and the plate decreased. However, for the cylinder location at the same level or downstream from the plate trailing edge, there were regions of essentially larger oscillation amplitude compared to an isolated cylinder case. Maximum amplitude growth by 39% was observed.

© 2021 Elsevier Ltd. All rights reserved.

## 1. Introduction

A phenomenon of self-exciting oscillations of elastic, or elastically mounted rigid bluff bodies immersed in a fluid flow, known as vortex-induced vibrations (VIV), may be observed near chimneys, submarine pipelines, risers, etc. (Païdoussis et al., 2010). When a structural natural frequency is close to von Karman street frequency, resonant oscillations take place. The body experiences a periodic force due to vortex shedding and oscillates, mostly in the traversal direction relative to the flow. VIV occur in a certain velocity range (so-called synchronization or lock-in range), where the vortex shedding frequency (as well as the oscillation frequency) is not governed by Strouhal law but is close to the natural frequency of the cylinder. VIV can lead to fatigue damage accumulation up to the destruction of the structure, but they can also be used to harvest electric energy from the kinetic energy of air or water flow.

VIV studies have a long history. The first classical experiments were conducted by Feng (1968), who performed tests on the cross-flow vibrations of an elastically mounted cylinder in a wind tunnel. Two branches (later called the *lower* and *initial* branches) of response connected by a hysteresis loop were found. Brika and Laneville (1993) and Khalak and Williamson (1999) explained jumps in vibration amplitude by restructuring of the oscillating cylinder's wake. Williamson and Roshko (1988) found two regular vortex shedding modes for a freely vibrating cylinder: 2S, when two single vortices shed from the cylinder per cycle, and 2P, when two pairs of vortices shed per cycle. Subsequent studies of Khalak and Williamson (1996, 1999) showed that another branch exists for lower mass ratio (ratio of the cylinder mass to the displaced fluid mass), which was called *upper*; it corresponds to larger vibration amplitudes (nearly one cylinder diameter  $D$ ).

\* Corresponding author.

E-mail address: [ivanov@imec.msu.ru](mailto:ivanov@imec.msu.ru) (O. Ivanov).

Zhou et al. (1999) numerically showed that adding a streamwise degree of freedom (DOF) to the cylinder increases the maximum amplitude compared to 1-DOF vibration. As a vivid confirmation of this finding, Jauvtis and Williamson (2004) discovered a *super-upper* branch for 2-DOF cylinder for mass ratios less than 6. The vibration amplitude is nearly 1.5D; two triplets of vortices are formed per cycle of the body motion (named 2T mode). Further details of the VIV phenomena for different types of isolated vibrating cylinders (flexible, tapered, pivoted, elliptic, etc.) can be found in Parkinson (1989), Sarpkaya (2004), Williamson and Govardhan (2004), Bearman (2011), Kumar et al. (2018), and in the books of Paidoussis et al. (2010) and Fredsoe and Mutlu Sumer (2006).

It is known that the proximity of a plane boundary significantly changes the flow near a rigid cylinder. The gap ratio  $G/D$  and relative boundary layer thickness  $\delta/D$  (or velocity profile if the cylinder is immersed in the boundary layer) become important. Flow around a fixed circular cylinder near a plane boundary, including pressure distributions over the cylinder and the plane and flow characteristics for gaps from 0 to  $3.5D$  were studied by Bearman and Zdravkovich (1978), and vortex suppression for a gap ratio less than 0.3 was observed. The flow around a cylinder near a plane with a laminar boundary layer was also investigated by Price et al. (2002) through particle image velocimetry (PIV); they obtained regular vortex shedding only for  $G/D \geq 0.5$ , however, for smaller gap ratios, a periodicity of the flow (without vortex shedding) was observed. A similar threshold was obtained by Lin et al. (2009) in PIV measurements: regular and alternating vortex shedding is suppressed for  $G/D < 0.5$ , but main shedding frequency can be detected up to  $G/D = 0.3$ . The influence of the boundary layer on vortex shedding from a fixed cylinder was examined by Grass et al. (1984) and Lei et al. (1999).

The VIV studies of a cylinder near a plane, both for 1-DOF and 2-DOF cases, show a complicated response to the proximity of the boundary. It may be expected that the presence of a plane boundary will depress VIV because of suppressed vortex shedding around a fixed cylinder. However, Fredsoe et al. (1987) found that “one-side” vibration amplitude and corresponding synchronization range of reduced velocities  $V_r = V/(f_N D)$  ( $V$  is the freestream velocity and  $f_N$  is the cylinder’s natural frequency) increase with the gap decrease. Yang et al. (2009) obtained similar results: amplitude was nearly constant for intermediate gaps and reached the maximum value at minimal measured gap  $G/D = 0.06$ . It was found that for small gaps ( $G/D = 0.06$  and  $0.3$ ), the vibration frequencies  $f/f_n$  (where  $f_n$  is the natural frequency of the cylinder) are noticeably larger than for other gaps at the same reduced velocities. Wang et al. (2013) observed a reduction of amplitude  $A$  with a reduction of the gap ratio, but a further increase of  $A$  for  $G/D \leq 0.15$  due to the bounce-back effect. Zang and Zhou (2017) investigated VIV in the gap ratio range 0.05–1.5 and found similar but strictly monotonous behavior of amplitude for all  $G/D$ . In numerical simulations of 2-DOF VIV, Zhao and Cheng (2011) and Chung (2016) studied the effect of bounce-back of the vibrating cylinder and reported intensive VIV and vortex shedding for very small gap ratios ( $G/D = 0.002$  and  $0.06$ , respectively). Different wake vortex modes were observed: (2S, 2P) by Chung (2016) and (2S, 2P, 2T) by Zhao and Cheng (2011) for different reduced velocity ranges. It is important to note that in all considered studies, irrespective of the change in “one-side” vibration amplitude, the mean amplitude of the cylinder near a rigid boundary was smaller than that of an isolated cylinder. A local increase of “one-side” amplitude for small gap ratios observed by Fredsoe et al. (1987), Yang et al. (2009), Zhao and Cheng (2011), and Chung (2016) corresponds to a larger “positive” amplitude  $A^+$  (the cylinder moves from a position of equilibrium away from the boundary) but smaller “negative” amplitude  $A^-$  (the cylinder moves from a position of equilibrium toward the boundary) that was nearly equal to the gap size, while the mean amplitude  $A_{mean} = (A^+ + A^-)/2$  is always less than amplitude  $A_0$  for an isolated cylinder.

In recent decades, VIV application in energy harvesting has been intensively investigated. There are many concepts of bodies oscillating in moving fluid, e.g., flapping flaps and airfoils, vibrating cantilever plates, and elastically mounted cylinders and cables used in energy harvesting. Depending on the magnitude of vibration amplitude, induction coils and magnets, and capacitive or piezoelectric transducers are utilized to convert mechanical energy to electrical (Li et al., 2016). Note VIVACE designed by Bernitsas et al. (2008) as a successful idea of an energy harvester based on oscillations of an elastically mounted cylinder.

The problem of increasing the efficiency of the energy generators and harvesters is very important. Energy harvesting leads to an additional damping in the vibrating system, resulting in the important problem of finding a way to intensify vibrations, because a VIV device can generate more power in a larger operating velocity range if the vibration amplitude of the body increases. One method to increase VIV amplitude is to place a rigid cylinder of the same diameter upstream to the elastically supported cylinder. In this case, a range of significant oscillation amplitude ( $A/D \sim 1$ ) is extended and the amplitude monotonically increases with reduced velocity growth (Assi et al., 2006). In this paper, a new amplification effect of vibration amplitude is discovered; namely, the amplitude of a vibrating elastic cylinder located in proximity to a trailing edge of a rigid plate is noticeably larger than that of an isolated cylinder.

Note that VIV studied in this paper are essentially three-dimensional: the cylinder is, in fact, a string with a circular cross-section, which oscillates in the first mode in all regimes considered in this study. However, due to its large aspect ratio, it is natural to expect that the effect of increasing amplitude near a finite-length plate will remain in a purely two-dimensional problem.

The paper is organized as follows. In Section 2, we describe the experimental apparatus and the model used in the tests. Section 3 is devoted to results for an isolated cylinder and comparison with previously known data. In Section 4, we present results for a cylinder near a rigid finite-length plate. Finally, Section 5 summarizes the results and concludes the paper.

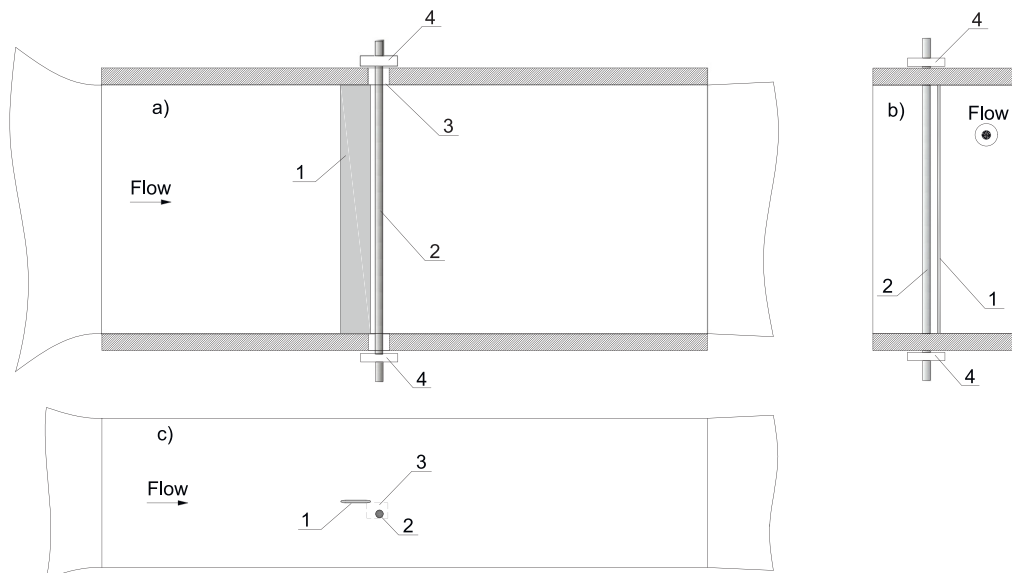


**Fig. 1.** Wind tunnel test section: side view (a), cross-section view (b), top view (c). 1 – plate, 2 – rubber cylinder, 3 – holes in test section walls, 4 – clips fixing cylinder. Plate and cylinder are shown with a larger scale.

## 2. Experimental setup

The experiments were conducted in a wind tunnel A-4 of the Institute of Mechanics, Lomonosov Moscow State University. The test section (Fig. 1) was 500 mm in height, 300 mm in width, and 1200 mm in length. The constriction ratio of the wind tunnel was 36:1. The side and upper walls had technological windows to observe and measure vibration amplitude and for visualization purposes. A rubber cylinder (cord) with a round cross-section was spanned vertically through the holes in 34 mm plexiglass walls of the test section and fixed by clips so that the actual cylinder length was  $L = 568$  mm. The unloaded cylinder diameter was 6.6 mm; after stretching, the diameter decreased to  $D = 6.0$  mm. The first natural frequency of the cylinder in still air could be calculated with high accuracy as for a string with fixed ends in a vacuum:  $f_N = (2L)^{-1} \sqrt{\sigma/\rho}$ , where  $\sigma$  is the string tension stress, and  $\rho$  is its density.

The plate was mounted at the zero angle of attack; its leading edge was nearly 50 cm downstream from the test section inlet and shifted by 3 cm in a transverse direction from the vertical midplane. The plate was 35 mm long (streamwise direction), 2 mm thick, its edges were ellipse-shaped with 6 and 2 mm axes. The position of the rubber cylinder center in the main series of experiments was changed from 6 mm (1D) upstream to 12 mm (2D) downstream relative to the plate's trailing edge and shifted by 0–14 mm (0–2.3D) in the traverse direction from the plate.

The vibration amplitude and frequency were measured at the cylinder antinode by laser triangulation sensor Riftek RF-603 mounted in a plane of oscillations (Fig. 2). Air velocity was in the range of 0.4–0.65 m/s and was measured by wind anemometer RZ GM8903. The corresponding Reynolds number based on the cylinder diameter was 180–260. The vortex shedding frequency was measured by the DISA constant temperature anemometer (CTA) 55D05 with hot-wire probe 55P81. To visualize the flow around the cylinder, a laser sheet produced by a continuous 532 nm wavelength green laser and smoke generator were used. The flow pictures were received by high-speed camera Allied Vision Bonito CL-400B. The scheme of visualization is shown in Fig. 2.

## 3. Damping and VIV of an isolated cylinder

### 3.1. Damping coefficient measurements

A simple model to describe cylinder's transverse motion in the first mode is

$$m \frac{d^2 y}{dt^2} + c \frac{dy}{dt} + ky = F(t), \quad (1)$$

where  $y$  is the traverse coordinate of the cylinder center,  $m$  is the structural mass,  $c$  is the structural damping,  $k$  is the spring constant, and  $F(t)$  is the fluid force acting in the transverse direction. With good accuracy (Williamson and Govardhan, 2004), it may be assumed that  $y = A \sin(\omega t)$  and  $F = F_0 \sin(\omega t + \phi)$ . Added mass force is neglected because in the case of air flow, its magnitude is three orders less than the inertial force ( $m^* = m_{cylinder}/m_{air} \gg 1$ ).

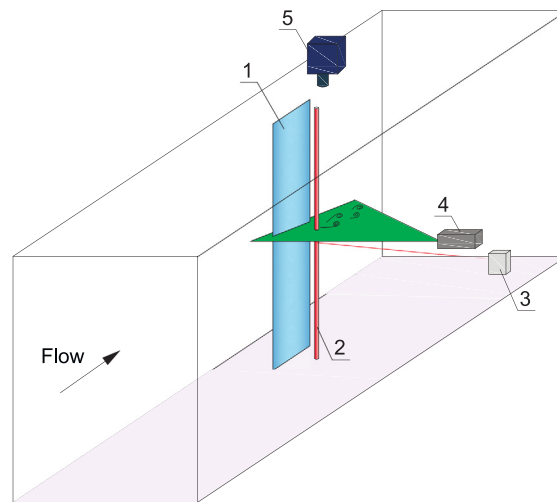


Fig. 2. Scheme of measurements and the flow visualization. 1 – plate, 2 – rubber cylinder, 3 – laser triangulation sensor, 4 – laser, 5 – camera.

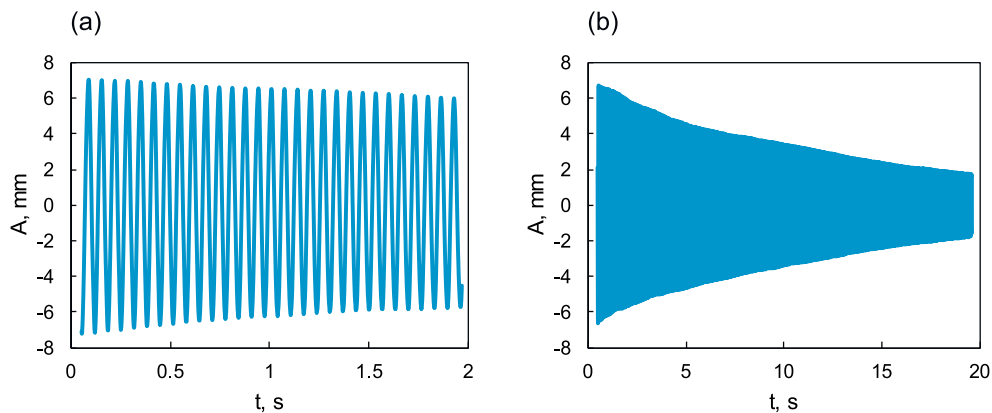
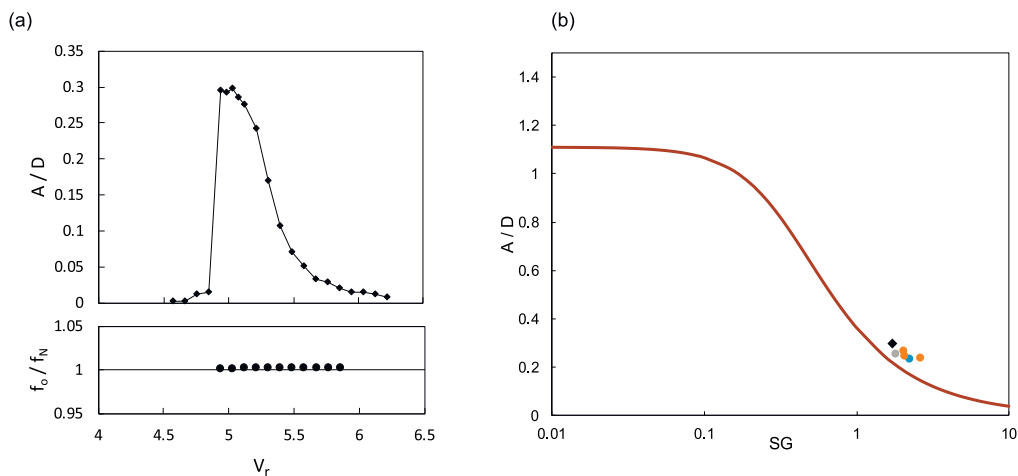


Fig. 3. Decay of the cylinder oscillations with time during (a) 2 s; (b) 20 s.

Considering damped oscillations in the absence of the air flow and by matching them with Eq. (1), one of the governing parameters of the problem could be measured: damping ratio  $\zeta = c/(2\sqrt{km})$ . To this end, a series of free vibration tests was conducted. For several values of tension, initial excitation was introduced, and displacement of the cylinder center versus time was measured (Fig. 3). From 20-s samples, structural damping and damping ratios were extracted by the least squares method. Several rubber materials and end clamping conditions were tested, and the one with the lowest damping ratio  $\zeta = 1.4 \times 10^{-3}$  was chosen for the present experiments. The corresponding Skop–Griffin parameter (Skop and Griffin, 1973) for an isolated cylinder  $SG = 2\pi^3 St^2 m^* \zeta = 1.7$  (taking into account that the Strouhal number  $St$  in the experiments was nearly 0.2).

### 3.2. VIV of an isolated cylinder

The first series of air-on experiments was performed with an isolated cylinder, i.e., without the plate installed. The cylinder's tension was set so that the first natural frequency  $f_N = 15.05$  Hz corresponded to the velocity of VIV onset, which was in the range of wind tunnel and anemometer operation. A typical cylinder vibration amplitude ratio  $A/D$  and the oscillation frequency versus  $V_r$  are shown in Fig. 4a. The Reynolds number range corresponding to the response region was 180–210. The oscillation frequency  $f_o$  remained almost unchanged for all  $V_r$ :  $f_o/f_N = 1$  with high accuracy (Fig. 4a). In the present experiments, the maximum vibration amplitude  $A/D = 0.30$  was obtained. As can be seen in Fig. 4b, the peak amplitudes were quite well correlated with the Griffin plot (Skop and Griffin, 1973). As our experiments were conducted in air flow, the Skop–Griffin parameter was quite large so that the peak  $A/D$  value is three times lower than the asymptotic value as  $SG \rightarrow 0$ . To increase the peak amplitude of an isolated cylinder, one should decrease the value of  $SG$ ; given that  $St \approx 0.2$ , this is possible either by lowering the damping ratio, or lowering the mass ratio  $m^*$ . However,



**Fig. 4.** (a) typical oscillation amplitude of an isolated cylinder (upper figure) and the oscillation frequency (lower figure) versus reduced velocity; (b) the experimental  $A/D$  values with the present rubber cylinder for different tensions and end fixing (points) at the Griffin plot (line).

the damping ratio for rubber and other elastomers is limited from below by the internal material damping. The decrease of the mass ratio  $m^*$  (in our experiments  $m^* \approx 1140$ ) is possible only by using a hollow cylinder or foamed materials, or by changing fluid properties, e.g., by using water instead of air flow. As this research is aimed at wind energy generation, we studied VIV in air so that  $SG$  was limited from below, and the peak  $A/D$  ratio obtained in this series of tests was nearly the maximum that could be obtained in air-flow conditions for non-hollow rubber cylinders of the given length. The experiments discussed below correspond to tension and end clamping conditions shown for an isolated cylinder by diamond mark in Fig. 4b.

VIV significantly affects the wake behind the cylinder. Namely, when the vortex shedding frequency  $f_v$  becomes close to the natural frequency  $f_N$ , the VIV appears and lock-in phenomenon occurs: in a certain velocity range, the vortex shedding frequency  $f_v$  is not governed by the relation  $St \approx 0.2$  (Strouhal law), but equals  $f_o = f_N$ . To measure  $f_v$  in experiments, the CTA probe was located at  $0.5D$  in the transversal direction and  $3D$  downstream from the mean location of the cylinder center. The ratio  $f_v/f_N$  for elastic and rigid cylinders of identical diameters is shown in Fig. 5. Outside the lock-in range, both relations are close to the line  $St = (f_v/f_N)/V_r = 0.2$ , but start to slightly deviate for  $V_r > 6.5$ . The wake structures are similar for oscillating and non-oscillating cases, as demonstrated by smoke visualization in Fig. 6. They correspond to 2S mode in the classification of Williamson and Roshko (1988).

#### 4. Cylinder near a finite-length plate

It is known that the proximity of the infinite-length plane wall significantly changes the flow structure near both oscillating and non-oscillating cylinders. In the studies discussed in Section 1, the decrease of amplitude was obtained for the intermediate gap ratio, and both a decrease and a local increase (mainly due to the bounce-back effect) of “one-side” amplitude was observed by different authors for  $G/D \leq 0.3$ . It was expected that the flow would be more complicated if the solid boundary was reduced to a finite-length plate. The authors of the present paper are not aware of any studies in which a cylinder oscillates near a rigid finite-length plate. The closest problem formulations are the studies of the interaction between an airfoil and the cylinder, which usually consider a dynamic response in the system of a flapping airfoil and a stationary or vibrating cylinder (Derakhshandeh et al., 2016; Zhang et al., 2017).

In our experiments, an elastic cylinder was located near the trailing edge of a plate mounted at a zero angle of attack. Two parameters of the cylinder position were used (Fig. 7): spacing  $S$  was the streamwise distance between the cylinder center and the plate trailing edge, and gap  $G$  was the distance between the cylinder surface and the plate. We assumed that  $S < 0$  if the cylinder center was located upstream relative to the plate trailing edge. For each location of the cylinder, the flow speed was tuned to reach a maximum of  $A/D$  curve, which in all regimes looked similar to Fig. 4a. This maximum value was then compared to the relative maximum amplitude  $A_0/D$  for an isolated cylinder (without the plate).

##### 4.1. Vibration amplitudes

The plate edge proximity strongly affected the vibration amplitude. When the cylinder was located at  $S/D = -2$  (far upstream from the plate’s trailing edge), the maximum of  $A/D$  decreased and the lock-in range shifted to higher reduced velocities with a decrease of  $G/D$  (Fig. 8a). Similar behavior of these curves was observed by Fredsoe et al. (1987) and Yang et al. (2009). In the case of the cylinder center located slightly downstream relative to the plate,  $S/D = 0.5$  (Fig. 8b), the

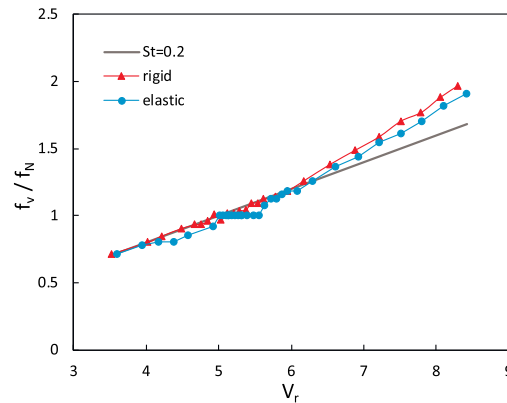


Fig. 5. The vortex shedding frequencies for an elastic cylinder and a rigid cylinder. Solid line corresponds to  $St = 0.2$  ( $f_v/f_N = 0.2V_r$ ).

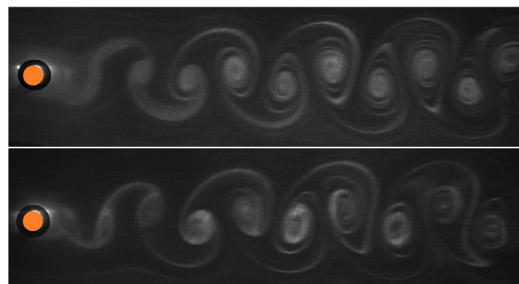


Fig. 6. Flow visualizations near an oscillating (upper figure,  $V_r = 5$ ) and a fixed (lower figure,  $V_r = 4.8$ ) cylinder.

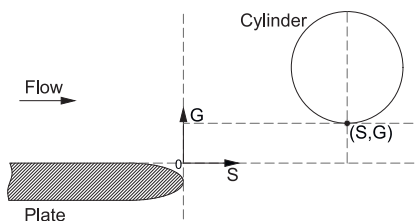


Fig. 7. A definition of the cylinder position by spacing  $S$  and gap  $G$ .

synchronization range became wider, and the maximum amplitude behavior changed to the opposite: it increased with a reduction in the gap ratio. The variation of the streamwise position of the cylinder for the constant gap ratio  $G/D = 0.5$  is shown in Fig. 8c and clearly indicates the existence of a global maximum of the vibration amplitude in close proximity to the plate's trailing edge.

Fig. 9 shows maximum oscillation amplitudes  $A$  rated to the same value for an isolated cylinder  $A_0$  at lines  $S = const$ . It is seen that for  $G/D \geq 2$ , the  $A/A_0$  ratio was close to 1, i.e., the oscillating cylinder did not “feel” the presence of the plate, and the interaction between the plate and the cylinder wakes vanished; this is in agreement with the results of Lei et al. (1999) for a fixed cylinder. For smaller values of  $G$ , the effect of the plate proximity essentially depended on  $S$ . For the cylinder located sufficiently far upstream from the plate's trailing edge,  $S/D \leq -1$ , the plate effect was negative:  $A/A_0 < 1$ , i.e., the maximum oscillation amplitude decreased for closer plate location. The same effect was obtained in Wang et al. (2013) and Zang and Zhou (2017) on cylinder oscillation near an infinite-length plane. But for  $S/D \geq -0.5$ , there was a range of gaps where oscillations were amplified compared to the case of an isolated cylinder. At  $S/D = -0.5$ , maximum amplification  $\alpha = (A/A_0 - 1) \times 100\%$  reached nearly 7% at the gap  $G/D = 0.85$ , and further downstream the  $G$  range of amplified vibrations increased in size and magnitude. The maximum value of  $\alpha = 39.2\%$  was obtained at  $G/D = 0.08$ ,  $S/D = 0.5$ , i.e., at the plate's trailing edge located on almost the same streamwise level as a front point of the cylinder surface. A further increase of  $S$  led to the reduction of the effect up to negative  $\alpha$  near the plate wake, but the zone of positive  $\alpha$  still existed and moved in the direction of larger values  $G/D = 0.5 - 1$ .

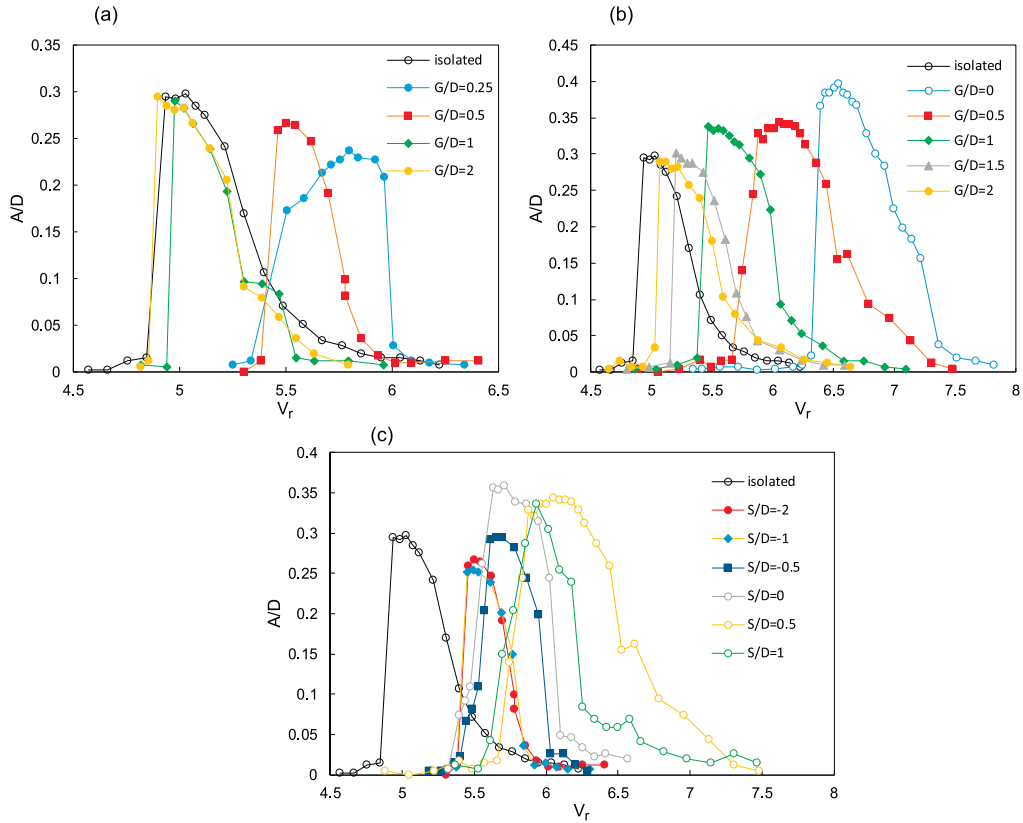


Fig. 8. Vibration amplitude  $A/D$  versus reduced velocity  $V_r$ . (a) line  $S/D = -2$ ; (b) line  $S/D = 0.5$ ; (c) line  $G/D = 0.5$ .

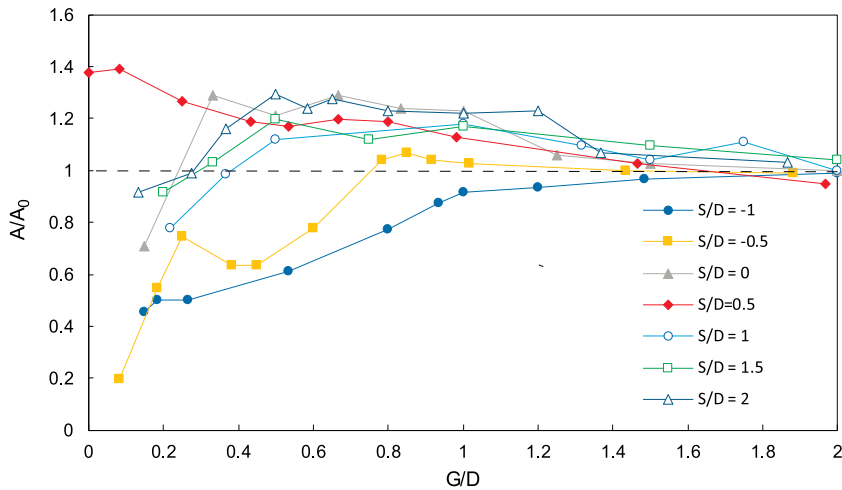


Fig. 9. Relative vibration amplitude  $A/A_0$  for different  $S$ .

All measured values of  $A/A_0$  are brought together in the form of a heat map in Fig. 10. There were two regions of considerable positive plate effect. The first was located above and just downstream from the plate's trailing edge. The second region was located further from the plate's edge in both directions: for  $G/D = 0.3 - 1.2$  and  $S/D > 1.5$ .

It is important to note that the plate proximity does not distort the trajectory of the cylinder oscillations: a motion of antinode was sinusoidal for all cylinder locations, and the oscillation frequency  $f_o$  was almost independent from  $S$ ,  $G$ , and reduced velocity (maximum of  $|f_o/f_N - 1| < 0.003$ ). No bounce-back of the cylinder was observed in the experiments, in contrast to the studies of Yang et al. (2009) and Zhao and Cheng (2011). To illustrate these statements, a time series of

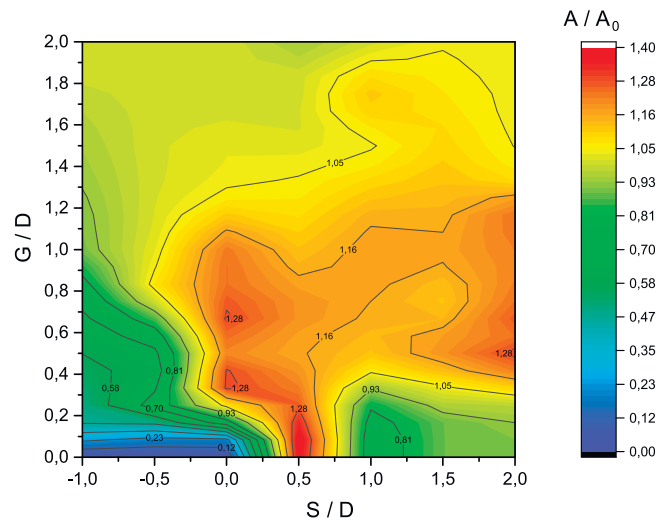


Fig. 10. Vibration amplitude  $A$  of a cylinder near a plate rated to the reference one  $A_0$  for an isolated cylinder as a function of  $S$  and  $G$ .

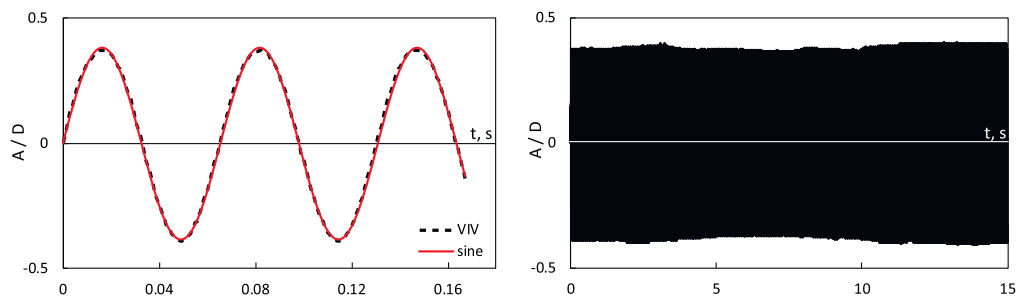


Fig. 11. A time series of VIV at  $S/D = 0.5$ ,  $G/D = 0$ : (a) comparison of the experimental data with sine; (b) cylinder deflection for a time range of 15 s.

VIV at  $S/D = 0.5$ ,  $G/D = 0$  is shown in Fig. 11: a trajectory of the cylinder is symmetrical, just slightly different from a sine, and VIV amplitude is nearly a constant.

#### 4.2. Smoke visualizations

Smoke visualizations of the flow were conducted for several flow regimes. In Fig. 12, three pairs of flow visualizations are shown in the case of the cylinder located at  $S/D = -2.2$  and three  $G/D$  ratios: 2.4, 1, 0.33. The values of the reduced velocity  $V_r$  corresponding to vibration (maximum amplitude) and non-vibration (smaller, out of the lock-in range, reduced velocity) cases are provided in Table 1. The upper regime with  $G/D = 2.4$  (Fig. 12a) corresponds to the maximum cylinder amplitude with  $A/D = 0.29$  at  $V_r = 4.8$  and the topmost position of the cylinder during vibration. Fig. 12b corresponds to  $V_r = 4.2$ ; the absence of vibrations is confirmed by amplitude measurements (measured  $A/D \sim 0.003$  is of the order of magnitude of the sensor sensitivity), and the corresponding vortex shedding frequency was less than the natural frequency (see Section 4.3). It is seen that wake structures were identical up to small distortions in vortices. One can see pairs of vortices shedding from the cylinder and, simultaneously, a chain of forming Kelvin–Helmholtz rolls of the plate wake for both regimes. Visualization of flow near an isolated plate shows that the flow around it was unseparated, and the plate wake stayed steady and laminar at least for  $20D$  downstream from the trailing edge. Hence, the perturbation of the plate wake and its quick breakdown occurred not due to instability of the plate wake itself, but due to the presence of vortices shed from the cylinder.

Reducing the gap ratio to  $G/D = 1$  changed the vortex shedding character (Fig. 12c, d): the counterclockwise rotating vortex had a worse condition to origin, and its vorticity and size were smaller than for a clockwise rotating vortex. The joint wake of the cylinder and the plate was wider for the oscillating cylinder. In both regimes, there was a zone of low velocity between the plate vortices and cylinder vortex pairs. A further decrease of the gap ratio to  $G/D = 0.33$  (Fig. 12e, f) led to the disappearance of the counterclockwise rotating vortex, which is in accordance with Bearman and Zdravkovich (1978). There remained only two vortices in the wake: the first from the cylinder and the second from the plate.

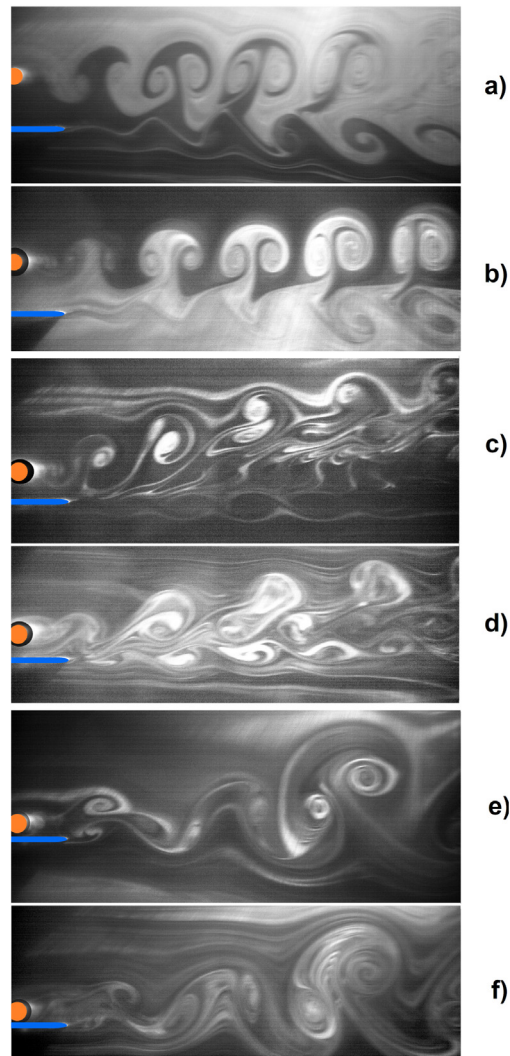


**Fig. 12.** Comparison of flow regimes around the cylinder (orange) and the plate (blue) for  $S/D = -2.2$ . Gap ratios  $G/D = 2.4$  (a, b), 1 (c, d), 0.33 (e, f). The case of vibrations (a, c, e) and non-vibrations (b, d, f). Corresponding reduced velocities are summarized in [Table 1](#).

**Table 1**

$V_r$  values corresponding to [Fig. 12](#).

$G/D$	Vibration case		Non-vibration case	
	Subfigure	$V_r$	Subfigure	$V_r$
2.4	a	4.8	b	4.2
1	c	5	d	4.84
0.33	e	5.9	f	5.1

At  $S/D = 0.5$  and  $G/D = 0$ , the cylinder had the amplitude  $A/D = 0.38$  increased with respect to the isolated cylinder ( $A/A_0 = 1.27$ ); visualization of this flow regime is shown in [Fig. 13](#). The vortex structures for oscillating and non-oscillating cases were similar in general, but the counter-clockwise rotating vortices was weaker in the non-oscillating case. Note that there was no visible development of roll-up vortices past the plate.

The observed regimes of vortex shedding were somewhat similar to the 2S and S + P regimes ([Williamson and Roshko, 1988](#)) for an isolated cylinder, but not the same due to the presence of the plate. The vortex shedding regimes can be classified in terms of the single vortices (S) shed from the cylinder and the Kelvin-Helmholtz vortices (KH) located behind the plate. The regimes are shown in [Fig. 14](#). Three scenarios were observed. The first was related to almost all cases with  $S/D > 0$ , where the plate distorted the cylinder wake, but shedding scheme 2S ([Fig. 14a](#)) remained unchanged. A similar vortex shedding regime was observed for  $S/D < 0$  and large  $G/D$ : the cylinder did not affect the flow near the plate so

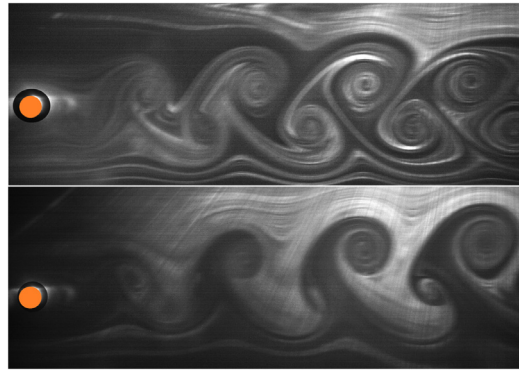


**Fig. 13.** Comparison of flow regimes,  $S/D = 0.5$ ,  $G/D = 0$ . Upper – oscillating cylinder,  $A/D = 0.38$ ,  $V_r = 6.6$ , lower – no oscillation,  $V_r = 6.2$ .

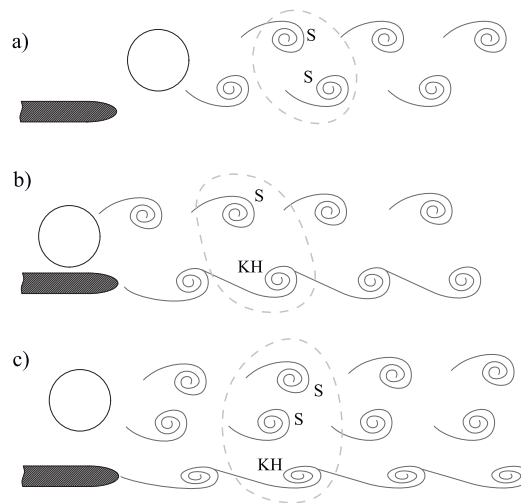


**Fig. 14.** Schemes of observed vortex shedding regimes: (a) 2S case; (b) S + KH case; (c) 2S + KH case.

that both cylinder and plate wakes did not distort each other. The second scheme S + KH (Fig. 14b) corresponds to small gaps: the plate wake broke down to a chain of KH vortices triggered by the cylinder wake, and one single vortex shed from the cylinder per oscillation period. In the case of the third regime (2S + KH, Fig. 14c), an intermediate gap allowed to shed two vortices from the cylinder per oscillation period, so the joint wake contained two S and one KH vortices.

#### 4.3. Vortex shedding frequencies

The vortex shedding frequency measurements were conducted in a separate series of experiments in a similar manner to an isolated cylinder (Section 3.2). The CTA probe was placed at the same position relative to the cylinder. As shown in the previous section, the presence of the plate shifted the lock-in range to higher reduced velocities. A similar action could be observed in frequency curves (Fig. 15): both for a rigid and an elastic cylinder, the vortex shedding frequencies  $f_v$  decreased when the cylinder was located closer to the plate. Fig. 15 provides evidence that the shift of the lock-in region is not due to vibrations, but only to the decrease of  $f_v$ .

### 5. Conclusions

Oscillations of a finite-span elastic cylinder near a finite-length rigid plate were investigated and compared to the case of an isolated cylinder. For cylinders located sufficiently upstream from the plate's trailing edge, the oscillation amplitude decreased when the gap between the cylinder and the plate decreased, which corresponds to the previously known results on infinite-length plates. For the cylinder location near or downstream from the plate's trailing edge, there existed regions of enlarged amplitude relative to the isolated cylinder case. A comprehensive experimental study of vibration amplitude for different cylinder locations with respect to the plate was performed. The greatest increase of the vibration amplitude was by 39% compared to the case of an isolated cylinder. Vortex shedding frequency measurements

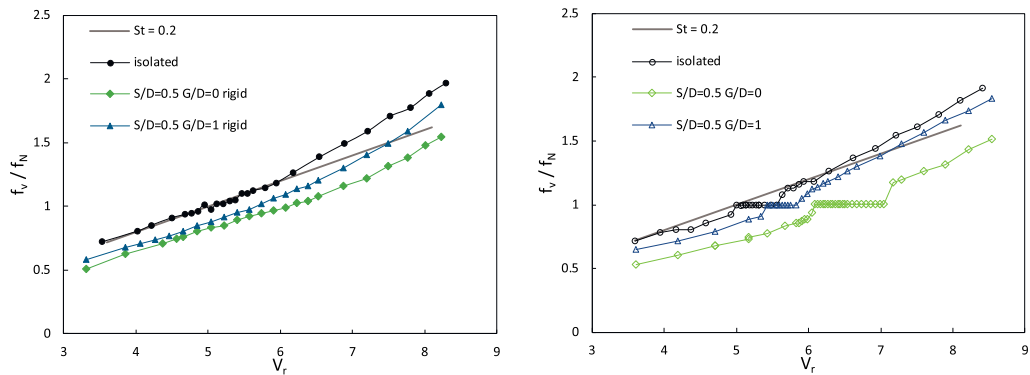


**Fig. 15.** Vortex shedding frequencies for a rigid (left) and an elastic (right) cylinder near the plate for  $S/D = 0.5$  and two gaps  $G/D = 0$  and 1, compared with an isolated cylinder curve. Solid line is  $St = 0.2$ .

and smoke visualizations of the flow for the cases of oscillating and non-oscillating cylinders were performed and showed no significant change of the flow structure for oscillating and non-oscillating cases.

It is worth noting that the considered oscillations did not belong to wake-induced vibrations, because the experiments with a plate without the cylinder show that its wake was steady and laminar. Hence, the only unsteadiness came from the cylinder, the vibrations of which were not induced by the plate wake. The presence of the plate modified the vortex shedding, but all dependencies remained qualitatively similar to an isolated cylinder case.

Note that the plate thickness ( $0.33D$ ) and the cylinder diameter  $D$  considered in this study were comparable. As the zone with  $A/A_0 > 1$  is located at the level or downstream from the plate's trailing edge (Fig. 10), the amplitude growth was related to the interaction of cylinder and plate wakes. Given that the plate wake thickness was of the order of the plate thickness, variation of the latter could affect the VIV amplitude. Hence, the analysis of the plate thickness effect can be a matter of future experiments devoted to the optimization of the  $A/A_0$  ratio.

The influence of the Reynolds number on the  $A/A_0$  growth is another interesting problem for future investigation. In this study, we considered a short Reynolds number range (180–260), so certain changes in results can be expected for larger Reynolds numbers.

Although the vibration growth in the presence of the finite-length plate is clearly seen, it is hard to reveal the amplification mechanism based only on the flow visualization; pressure measurements over the cylinder surface are necessary. As direct measurements on a rubber cylinder are difficult, a numerical study seems a more suitable option, which also can be a matter for a further study.

From a practical point of view, in energy harvesters based on the VIV of elastic cylinders, there is always a need for a rigid structure located close to the cylinder to arrange electricity generators, gauges, etc. This study shows that a specific configuration of such a rigid structure can also be efficient in terms of the increase in vibration amplitude and can be used to improve the efficiency of energy harvesting.

### CRedit authorship contribution statement

**Oleg Ivanov:** Conception and design of study, Acquisition of data, Analysis and/or interpretation of data, Writing – original draft, Writing – review & editing. **Vasily Vedenev:** Conception and design of study, Analysis and/or interpretation of data, Writing – original draft, Writing – review & editing.

### Declaration of competing interest

The authors declare that they have no known competing financial interests or personal relationships that could have appeared to influence the work reported in this paper.

### Acknowledgments

The authors are grateful to Sergey V. Guvernyuk for discussions of the problem and Alexander F. Zubkov and Anastasia B. Podoprosvetova for their technical support for the experiments. This work is supported by RFBR grant 18-31-20057 and by the Ministry of Science and Higher Education of the Russian Federation within the Program of “Supersonic” (agreement No. 075-15-2020-923).

All authors approved the version of the manuscript to be published.

## References

- Assi, G.R.D.S., Meneghini, J.R., Aranha, J.A.P., Bearman, P.W., Casaprima, E., 2006. Experimental investigation of flow-induced vibration interference between two circular cylinders. *J. Fluids Struct.* 22 (6–7), 819–827. <http://dx.doi.org/10.1016/j.jfluidstructs.2006.04.013>.
- Bearman, P.W., 2011. Circular cylinder wakes and vortex-induced vibrations. *J. Fluids Struct.* 27 (5–6), 648–658. <http://dx.doi.org/10.1016/j.jfluidstructs.2011.03.021>.
- Bearman, P.W., Zdravkovich, M.M., 1978. Flow around a circular cylinder near a plane boundary. *J. Fluid Mech.* 89 (1), 33–47. <http://dx.doi.org/10.1017/S002211207800244X>.
- Bernitsas, M.M., Raghavan, K., Ben-Simon, Y., Garcia, E.M.H., 2008. VIVACE (Vortex Induced Vibration Aquatic Clean Energy): A new concept in generation of clean and renewable energy from fluid flow. *J. Offshore Mech. Arct. Eng.* 130 (4), 041101. <http://dx.doi.org/10.1115/1.2957913>.
- Brika, D., Laneville, A., 1993. Vortex-induced vibrations of a long flexible circular cylinder. *J. Fluid Mech.* 250, 481–508. <http://dx.doi.org/10.1017/S0022112093001533>.
- Chung, M.H., 2016. Transverse vortex-induced vibration of spring-supported circular cylinder translating near a plane wall. *Eur. J. Mech. B Fluids* 55, 88–103. <http://dx.doi.org/10.1016/j.euromechflu.2015.09.001>.
- Derakhshandeh, J.F., Arjomandi, M., Dally, B., Cazzolato, B., 2016. Flow-induced vibration of an elastically mounted airfoil under the influence of the wake of a circular cylinder. *Exp. Therm Fluid Sci.* 74, 58–72. <http://dx.doi.org/10.1016/j.expthermflusci.2015.12.003>.
- Feng, C.C., 1968. The Measurements of Vortex-Induced Effects in Flow Past Stationary and Oscillating Circular and D-Section Cylinder (Master's Thesis). University of British Columbia, Vancouver, B.C., Canada. <http://dx.doi.org/10.14288/1.0104049>.
- Fredsoe, Jorgen, Mutlu Sumer, B., 2006. *Hydrodynamics Around Cylindrical Structures (Revised Edition)*. Vol. 26. World Scientific.
- Fredsoe, J., Sumer, B.M., Andersen, J., Hansen, E.A., 1987. Transverse vibrations of a cylinder very close to a plane wall. *J. Offshore Mech. Arct. Eng.* 109 (1), 52. <http://dx.doi.org/10.1115/1.3256990>.
- Grass, A.J., Raven, P.W.J., Stuart, R.J., Bray, J.A., 1984. Influence of boundary layer velocity gradients and bed proximity on vortex shedding from free spanning pipelines. *ASME J. Energy Resour. Technol.* 106(1), 70–78. <http://dx.doi.org/10.1115/1.3231028>.
- Jauvtis, N., Williamson, C.H.K., 2004. The effect of two degrees of freedom on vortex-induced vibration at low mass and damping. *J. Fluid Mech.* 509, 23–62. <http://dx.doi.org/10.1017/S0022112004008778>.
- Khalak, A., Williamson, C.H.K., 1996. Dynamics of a hydroelastic cylinder with very low mass and damping. *J. Fluids Struct.* 10 (5), 455–472. <http://dx.doi.org/10.1006/jfls.1996.0031>.
- Khalak, A., Williamson, C.H., 1999. Motions, forces and mode transitions in vortex-induced vibrations at low mass-damping. *J. Fluids Struct.* 13 (7–8), 813–852. <http://dx.doi.org/10.1006/jfls.1999.0236>.
- Kumar, D., Mittal, M., Sen, S., 2018. Modification of response and suppression of vortex-shedding in vortex-induced vibrations of an elliptic cylinder. *Int. J. Heat Fluid Flow* 71, 406–419. <http://dx.doi.org/10.1016/j.ijheatfluidflow.2018.05.006>.
- Lei, C., Cheng, L., Kavanagh, K., 1999. Re-examination of the effect of a plane boundary on force and vortex shedding of a circular cylinder. *J. Wind Eng. Ind. Aerodyn.* 80(3), 263–286. [http://dx.doi.org/10.1016/S0167-6105\(98\)00204-9](http://dx.doi.org/10.1016/S0167-6105(98)00204-9).
- Li, D., Wu, Y., Da Ronch, A., Xiang, J., 2016. Energy harvesting by means of flow-induced vibrations on aerospace vehicles. *Prog. Aerosp. Sci.* 86, 28–62. <http://dx.doi.org/10.1016/j.paerosci.2016.08.001>.
- Lin, W.-J., Lin, C., Hsieh, S.-C., Dey, S., 2009. Flow characteristics around a circular cylinder placed horizontally above a plane boundary. *J. Eng. Mech.* 135 (7), 697–716. [http://dx.doi.org/10.1061/\(asce\)0733-9399\(2009\)135:7\(697\)](http://dx.doi.org/10.1061/(asce)0733-9399(2009)135:7(697)).
- Païdoussis, M.P., Price, S.J., De Langre, E., 2010. *Fluid-Structure Interactions: Cross-Flow-Induced Instabilities*. Cambridge University Press.
- Parkinson, G., 1989. Phenomena and modelling of flow-induced vibrations of bluff bodies. *Prog. Aerosp. Sci.* 26 (2), 169–224. [http://dx.doi.org/10.1016/0376-0421\(89\)90008-0](http://dx.doi.org/10.1016/0376-0421(89)90008-0).
- Price, S.J., Sumner, D., Smith, J.G., Leong, K., Païdoussis, M.P., 2002. Flow visualization around a circular cylinder near to a plane wall. *J. Fluids Struct.* 16 (2), 175–191. <http://dx.doi.org/10.1006/jfls.2001.0413>.
- Sarpkaya, T., 2004. A critical review of the intrinsic nature of vortex-induced vibrations. *J. Fluids Struct.* 19 (4), 389–447. <http://dx.doi.org/10.1016/j.jfluidstructs.2004.02.005>.
- Skop, R.A., Griffin, O.M., 1973. A model for the vortex-excited resonant response of bluff cylinders. *J. Sound Vib.* 27 (2), 225–233. [http://dx.doi.org/10.1016/0022-460X\(73\)90063-1](http://dx.doi.org/10.1016/0022-460X(73)90063-1).
- Wang, X.K., Hao, Z., Tan, S.K., 2013. Vortex-induced vibrations of a neutrally buoyant circular cylinder near a plane wall. *J. Fluids Struct.* 39, 188–204. <http://dx.doi.org/10.1016/j.jfluidstructs.2013.02.012>.
- Williamson, C.H.K., Govardhan, R., 2004. Vortex-induced vibrations. *Annu. Rev. Fluid Mech.* 36, 413–455. <http://dx.doi.org/10.1146/annurev.fluid.36.050802.122128>.
- Williamson, C.H., Roshko, A., 1988. Vortex formation in the wake of an oscillating cylinder. *J. Fluids Struct.* 2 (4), 355–381. [http://dx.doi.org/10.1016/S0889-9746\(88\)90058-8](http://dx.doi.org/10.1016/S0889-9746(88)90058-8).
- Yang, B., Gao, F., Jeng, D.S., Wu, Y., 2009. Experimental study of vortex-induced vibrations of a cylinder near a rigid plane boundary in steady flow. *Acta Mech. Sinica* 25 (1), 51–63. <http://dx.doi.org/10.1007/s10409-008-0221-7>.
- Zang, Z., Zhou, T., 2017. Transverse vortex-induced vibrations of a near-wall cylinder under oblique flows. *J. Fluids Struct.* 68, 370–389. <http://dx.doi.org/10.1016/j.jfluidstructs.2016.11.021>.
- Zhang, G.Q., Ji, L.C., Hu, X., 2017. Vortex-induced vibration for an isolated circular cylinder under the wake interference of an oscillating airfoil: Part II. Single degree of freedom. *Acta Astronaut.* 133, 311–323. <http://dx.doi.org/10.1016/j.actaastro.2017.01.019>.
- Zhao, M., Cheng, L., 2011. Numerical simulation of two-degree-of-freedom vortex-induced vibration of a circular cylinder close to a plane boundary. *J. Fluids Struct.* 27 (7), 1097–1110. <http://dx.doi.org/10.1016/j.jfluidstructs.2011.07.001>.
- Zhou, C.Y., So, R.M.C., Lam, K., 1999. Vortex-induced vibrations of an elastic circular cylinder. *J. Fluids Struct.* 13 (2), 165–189. <http://dx.doi.org/10.1006/jfls.1998.0195>.